Mon. Not. R. Astron. Soc. **000**, 000–000 (0000) Printed 3 May 2006 (MN LATEX style file v2.2)

Separating cosmological B modes from foregrounds in cosmic microwave background polarization observations

Federico Stivoli[1], Carlo Baccigalupi[1,2,3,4], Davide Maino[5], Radek Stompor[6,7]
[1] *SISSA/ISAS, Astrophysics Sector, Via Beirut, 4, I-34014 Trieste, Italy*
[2] *INFN, Sezione di Trieste, Via Valerio 2, I-34014 Trieste, Italy*
[3] *Physics Division, Lawrence Berkeley National Laboratory, 1 Cyclotron Road, Berkeley, CA 94720, USA*
[4] *Institut für Theoretische Astrophysik, Universität Heidelberg, Albert-berle-Strasse 2, D-69120 Heidelberg, Germany*
[5] *Dipartimento di Fisica, Università di Milano, Via Celoria 16, I-20133, Milano, Italy,*
[6] *Computational Research Division, Lawrence Berkeley National Laboratory, 1 Cyclotron Road, Berkeley, CA 94720, USA*
[7] *Space Sciences Laboratory, University of California, Berkeley, CA 94720, USA*

3 May 2006

ABSTRACT

The detection and characterization of the B mode of Cosmic Microwave Background (CMB) polarization anisotropies will not be possible without a high precision removal of the foreground contamination present in the microwave band. In this work we study the relevance of the component separation technique based on the Independent Component Analysis (ICA) for this purpose and investigate its performance in the context of a limited sky coverage observation and from the viewpoint of a precise recovery of the B-mode power spectrum.

We focus on the low Galactic emission sky patch centered at 40 degrees in right ascension and -45 in declination, corresponding to the target of several operating and planned CMB experiments and which, in many respects, adequately represents a typical "clean" high latitude sky. We consider two combinations of low and high frequencies: 40, 90 GHz and 150, 350 GHz, where the main diffuse polarized Galactic signal is dominated by the synchrotron and thermal dust emissions, respectively. The foreground templates have been simulated in accordance with the existing observations in the radio and infrared bands, as well as the Wilkinson Microwave Anisotropy Probe (WMAP) and Archeops data. With the help of a parallel implementation of the FastICA code we explore a substantial parameter space varying Gaussian pixel noise level, observed sky area and the amplitude of the foreground emission, and conduct large Monte Carlo simulations to evaluate the errors and biases induced in the reconstruction for different choices of these variables. We identify a large subspace of this parameter space for which the quality of the CMB reconstruction is excellent. That includes the cases when the B mode CMB signal is up to a few times weaker than the foreground contamination and the noise amplitude comparable with the total CMB polarized emission. In these cases the error induced by the separation process is found to be comparable to or lower than the one from the cosmic variance and instrumental noise, and the biases much smaller than that. This performance is a result of the high spatial resolution and the high level of statistical independence between background and foreground emissions, as anticipated from the foreground models and the available observations. We also point out and discuss limiting cases of noise and foreground amplitude, when the ICA approach fails.

Although our analysis is limited by the absence of systematics in the simulated data, these results indicate that these component separation techniques could play a crucial role in the forthcoming experiments aiming at the detection of B modes in the CMB polarization.

E-mail: stivoli@sissa.it

Key words: methods – data analysis – techniques: image processing – cosmic microwave background.

1 INTRODUCTION

The main target of the planned probes for measuring the polarized component of the Cosmic Microwave Background (CMB) radiation is represented by the B modes, also known as "curl" component (Zaldarriaga, Seljak 1997; Kamionkowski et al. 1997), which are known to carry the imprint of primordial gravitational waves, as well as the weak lensing distortion induced by forming structures along the line of sight (Zaldarriaga, Seljak 1998).
The B signal in the CMB polarization is more than one order of magnitude smaller than the "gradient" mode (E) coming from all kinds of cosmological perturbations, and about two orders of magnitude lower if compared with the total intensity anisotropies (T) and their correlation with polarization (TE). The latter has been observed by WMAP on large angular scales (Kogut et al. 2003), while the E component has been observed by instruments operating on the ground (Kovac et al. 2002; Readhead et al. 2004). No glimpse of the B has been seen so far and it is apparent that its detection will represent an experimental challenge in terms of control of systematics and instrumental noise. An additional important limiting factor for these experiments is related to foreground emissions. In the frequency range going from 70 to 150 GHz the diffuse Galactic emission is known to be sub-dominant with respect to the total intensity CMB signal at medium and high Galactic latitudes. Though the knowledge of polarized foregrounds in the microwave band is still rather modest, and, apart of the recent Archeops observations (Benoit et al. 2004), usually based on the difficult extrapolations from the other distant frequency bands (Baccigalupi et al. 2001; Giardino et al. 2002), the weakness of the cosmological B signal makes the foreground contamination potentially and, almost certainly, very important for the recovery of this component everywhere in the sky and at any frequency (Baccigalupi 2003).

In this context, it is crucial to develop reliable data analysis tools which are capable of cleaning the CMB emission from the foreground contamination. Algorithms of this kind belong to the category of the component separation techniques. Those are designed to utilize multi-frequency information to separate emissions observed in the same frequency bands but produced by different physical processes. If robust prior knowledges are available about the signal to recover, the maximum entropy method (Hobson et al. 1998; Stolyarov et al. 2002) or Wiener filtering (Tegmark, Efstathiou 1996; Bouchet et al. 1999) may be implemented. On the other hand, in the case of CMB polarization, the polarized foregrounds are likely to be greatly uncertain, and a different approach, not relying on those priors, may be required. The class of "blind" component separation techniques exploits the statistical independence of the sky signals to be separated, a natural expectations for the CMB and Galactic emissions.
Among the techniques in this category, the Independent Component Analysis (ICA) has been considered in several works concerning component separation (Amari, Chichocki 1998; Hyvärinen 1999). It was first exploited as a neural network, i.e. capable of self-adjusting on time varying data streams (Baccigalupi et al. 2000), and then optimized in its fast form (FastICA) operating on an instrument with nominal features corresponding to the Planck experiment (Maino et al. 2002). It has been successfully tested on the real data from COBE/DMR (Maino et al. 2003), recovering the main CMB results of that experiments, concerning the amplitude and power spectrum of the cosmological perturbations on large scales. A flexible version of the ICA algorithm, capable to exploit available priors, has been proposed (Delabrouille et al. 2003). Recently, the FastICA algorithm was applied to simulated Planck data in polarization on all sky (Baccigalupi et al. 2004).

In the forthcoming years, the detection of the B modes will be attempted by balloon and ground based experiments, targeting sky regions where the foreground emission in total intensity is known to be low. One of those regions is centered on the position $(40^\circ, -45^\circ)$ in right ascension and declination. Such region has been observed by BOOMERanG 2K (Montroy et al. 2004), and is the target of the EBEx (Oxley et al. 2004) and QUAD (Bowden et al. 2004) experiments. As we shall see, even if the foreground emission is low in total intensity, it is relevant for the B modes of the CMB. In this work we test the FastICA performance in the reconstruction of the CMB polarized emission on that region of the sky, focusing on the recovery of B modes. Our work represents an exploratory study, and is not specialized for describing any operating or planned experiment. Our aim is to study if the blind component separation techniques have the capability to recover the B modes of the CMB on a patch of the sky, in presence of a substantial foreground contamination, as the latter occurrence might turn out to be true according to the existing studies concerning the Galactic emission. In section 2 we show how the background and foreground signals are simulated. In section 3 we describe how the angular power of the CMB polarization anisotropies is described on a limited portion of the sky. In section 4 we present a parallel version of the FastICA algorithm (lightICA) operating on polarization data; we apply it to the simulated sky signal realization and evaluate, biases and stability of the B mode reconstruction against variations in the background and noise realizations, noise and foreground fluctuation amplitude and extension of the sky area considered. Finally, in section 5 we discuss and summarize our results.

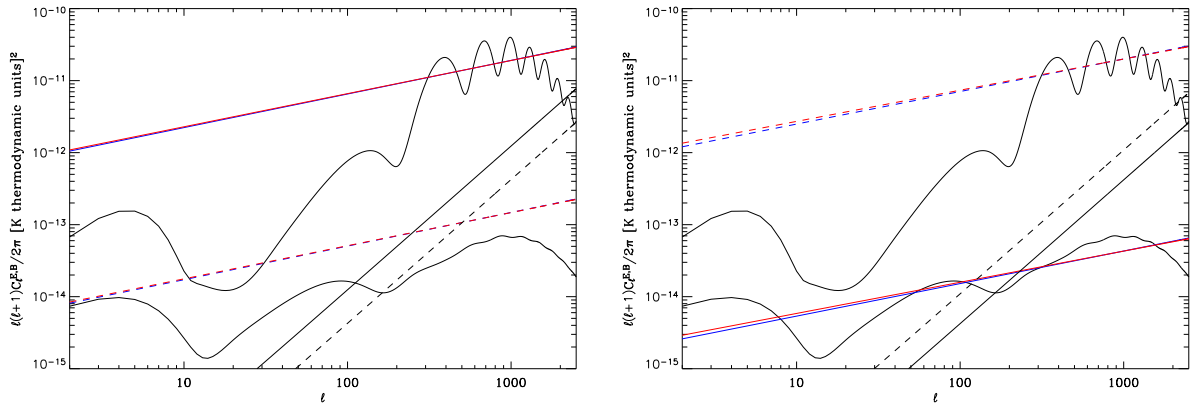

Figure 1. Power spectra of the different polarized sky signals relevant to the microwave observations. The almost flat straight lines represent the foreground contamination obtained by cutting out the Galactic plane up to $|b| = 50°$; the steep straight lines raising as l^2 represent the instrumental noise assumed in this work. The left and right panels represent the 40, 90 GHz and 150, 350 GHz frequency combinations, respectively. The solid lines represent the lowest frequency, while the dashed ones the highest one. These signals are plotted against the full sky CMB power spectra of anisotropies in thermodynamical units for E and B as assumed in this work (oscillating solid curves).

2 SIMULATED MAPS

The CMB emission is simulated accordingly to the cosmological concordance model (Spergel et al. 2003). The Hubble constant is H_0=72 km/s/Mpc, the overall geometry is flat, with a critical density made of baryons for a 4.4% fraction, 22.6% of Cold Dark Matter (CDM), and 73% of cosmological constant. The radiation component is made by photons and three massless neutrino species. The optical depth at reionization is fixed at $\tau = 0.11$. The perturbations are Gaussian, with a power spectrum characterized by a spectral index of scalar perturbations $n_s = 0.96$. The primordial gravity wave contribution is set to a 10% of the scalar perturbation amplitude, with a spectral index fixed accordingly to the single field inflationary model, $n_t = -n_s/6.8$. We include the contribution of lensing in the power spectrum, which is responsible for a substantial part of the power in the B modes of the CMB polarization anisotropies. The statistics of this component is non-Gaussian because of the correlation of different scales induced by lensing itself (Smith et al. 2004), and that could be exploited to separate it from the primordial tensor signal (Seljak, Hirata 2004). On the other hand, as we show in the next Section, on a limited patch of the sky as the one we consider here, the angular power spectrum for B is substantially affected by the leakage coming from the E modes, which are dominated by the primordial Gaussian statistics; therefore, in this work we assume that the entire B-modes signal is Gaussian. The power spectrum of CMB anisotropies is calculated using CMBFAST (Seljak, Zaldarriaga 1996) while the sky realizations have been obtained using the HEALPix package [1], assuming a Gaussian statistics. In antenna units, the CMB fluctuations at a frequency ν are obtained by the thermodynamical one by multiplying by the factor $x^2 \exp(x)/[\exp(x) - 1]^2$, where $x = h\nu/kT_{CMB}$, h and k are the Planck and the Boltzmann constant, respectively, while $T_{CMB} = 2.726$ K is the CMB thermodynamical units.

The polarized synchrotron emission has been simulated accordingly to two distinct recipes, which we summarize here. Both of them derived a template for the polarization angle θ by exploiting the observations in the radio band: these measures indicate a rather high fluctuation level interpreted as the effect of the small scale structure of the Galactic magnetic field (Uyaniker et al. 1999; Duncan et al. 1999), scaling as $C_l^\theta \sim l^{-2}$ on degree and sub-degree angular scale, up to the arcminute (Tucci et al. 2002), consistently also with recent observations at medium Galactic latitudes (Carretti et al. 2005). The template for the polarization angle was obtained by adopting the form above for C_l^θ, and assuming Gaussian distribution. The distinction between the two recipes is in the model assumed for the polarized intensity. In Baccigalupi et al. (2001), it was derived directly from the observations in the radio band including the existing data on large angular scale (Brouw, Spoelstra 1976). On the other hand, Giardino et al. (2002) exploited the all sky template of synchrotron in total intensity at 408 MHz (Haslam et al. 1982), assuming a theoretically synchrotron polarization fraction of about 75%; since the latter template has a resolution of about one degree or less, they completed the power on smaller scales by exploiting the total intensity observations in the radio band (Uyaniker et al. 1999; Duncan et al. 1999). The recipe adopted by Giardino et al. (2002) yields a stronger signal, and is what we take in this work as the polarized synchrotron template. In antenna units, the frequency scaling of the synchrotron is related to the energy distribution of electrons, exhibiting a steep power law as ν^{-3}, according to the observations of WMAP at intermediate and high Galactic latitude (Bennett et al. 2003).

[1] http://www.eso.org/science/healpix/

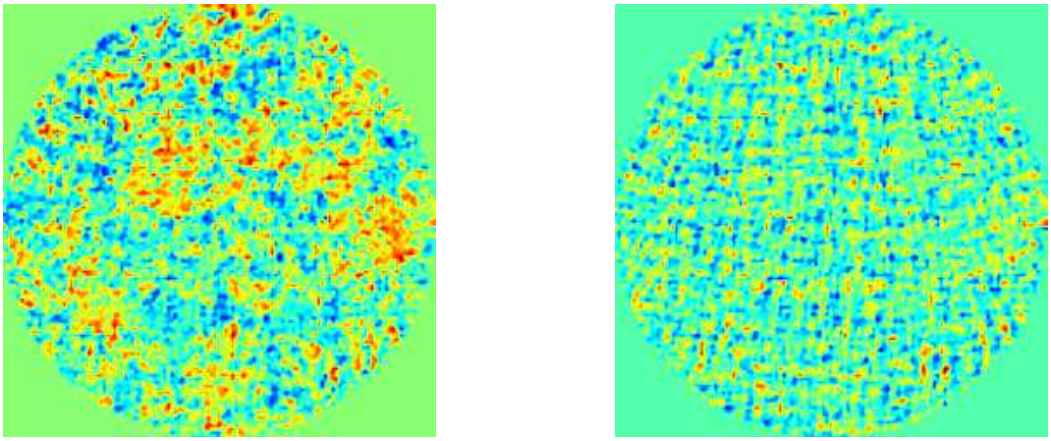

Figure 2. The total (CMB plus foregrounds) Q Stokes parameter emission in the sky area considered in this work, at 40 (left) and 90 GHz (right). At 90 GHz the signal appears dominated by the CMB signal, while the synchrotron contamination is evident at 40 GHz.

The polarized emission from the diffuse thermal dust has been detected for the first time in the Archeops data (Benoit et al. 2004), indicating a 5% polarization fraction with respect to the total intensity emission, which is very well known at 100μm and can be extrapolated at microwave frequencies (Finkbeiner et al. 1999). The pattern of the polarization angle is much more uncertain, and due to the magnetized dust grains which get locally aligned along the Galactic magnetic field (Prunet et al. 1998; Jones et al. 1995). Since the geometry and composition of the dust grains is still very uncertain, the simplest assumption is that the Galactic magnetic field is 100% efficient in imprinting the polarization angle pattern to the synchrotron and dust emission (Baccigalupi 2003).

These simulations indicate that the polarized foreground contamination is particularly challenging for the B mode CMB measurements, as this signal, arising only from the primordial gravitational waves and the weak lensing effect of the E polarization (Zaldarriaga, Seljak 1997, 1998), is about one order of magnitude smaller than the E component. On the other hand, the Galactic foregrounds are expected to have almost the same power in the two modes (Zaldarriaga 2001).
In figure 1 we show the contamination to the all sky CMB E and B spectra from the foreground emission corresponding to the synchrotron and dust diffuse Galactic signal after cutting out the Galactic plane up to $|b| = 50^\circ$, roughly corresponding to the latitudes considered in this work, as we explain below. The foreground power has been evaluated by fitting the actual sky signal with a power law, $C_l = \alpha l^\beta$. As it is evident, the models of the foreground emission indicate that the contamination to the B modes of the CMB is relevant in all cases. The lines raising as l^2 represent the levels of instrumental noise which we consider in this work, as we explain in detail in section 4. We do not consider the contribution from extra-Galactic point sources, yielding a spectrum raising approximately as l^2, with expected power below the noise level considered in this work (De Zotti et al. 1999).

We shall consider a circular top hat window with a radius $\theta_C = 10^\circ$ and 20°, corresponding to about 0.76% and 3.04% of the entire sky, respectively. The center in Galactic coordinates is at $l = 260^\circ$, $b = -62^\circ$, within the region considered by different experiments (Montroy et al. 2004; Bowden et al. 2004; Oxley et al. 2004). We take two frequency combinations, 40, 90 GHz, and 150, 350 GHz, where the dominant foreground emission is represented by the synchrotron and the thermal dust, respectively. The sky emission at the various frequencies, corresponding to the Q Stokes parameter, is shown in figures 2,3. At 90 and 150 GHz the CMB signal appears relatively free of foreground contamination, while at 40 and 350 GHz the foregrounds dominate. In Section 4 we describe more quantitatively the foreground CMB contamination by means of the angular power spectrum, defined formally in the next Section when a limited part of the sky is considered.

3 POLARIZATION PSEUDO POWER SPECTRA

In this work we apply the ICA component separation technique on a portion of the sky. We shall quantify the quality of the whole process in the angular domain, and thus it is relevant to describe the behavior of the angular power spectra when we cut out a part of the sky. As it is well known (see Chon et al. 2004, and references therein), on a finite portion of sky a transfer of power from the E to the B modes and vice versa occurs; for this reason, the angular power spectra get different from their values on all sky, and are called pseudo power spectra. Since the B modes are sub-dominant, the leakage from the power on E alters them substantially. In this paper we shall indicate the pseudo power spectra on E and B with $\tilde{C}_l^E$ and $\tilde{C}_l^B$, respectively, while the tilde is removed when we consider full-sky power spectra. For their calculation we adopt the recipe proposed by Hansen et al. (2002), which we exploit for calculating the $\tilde{C}_l^B$ spectra.

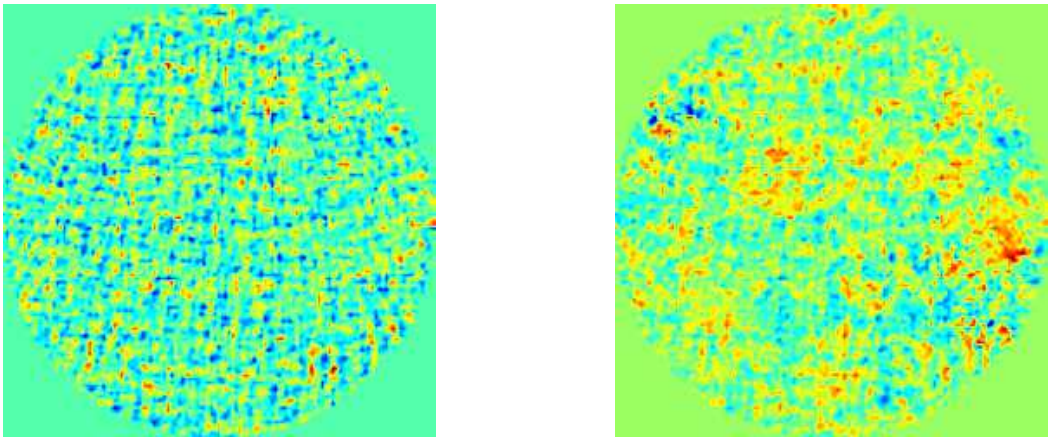

Figure 3. The total Q Stokes parameter emission in the sky area considered in this work, at 150 (left) and 350 GHz (right). At 150 GHz the signal appears dominated by the CMB emission, while the dust emission dominates at 350 GHz.

In order to consider the Fourier transform on a portion of the sphere, we apply a window function to the data set (Gabor 1946). The leakage between the polarization modes may be written as

$$\tilde{C}_l^E = \sum_{l'} C_{l'}^E K_2(l,l') + \sum_{l'} C_{l'}^B K_{-2}(l,l') \ , \tag{1}$$

$$\tilde{C}_l^B = \sum_{l'} C_{l'}^B K_2(l,l') + \sum_{l'} C_{l'}^E K_{-2}(l,l') \ , \tag{2}$$

where C_l^E and C_l^B are the polarization full-sky power spectra (Zaldarriaga, Seljak 1997), while the kernels $K_2(l,l')$ and $K_{-2}(l,l')$ depend on the form and the size of the cut, described by a generic function $G(\theta,\phi)$ which is zero in the sky regions which are not considered. The explicit expressions for the kernels are:

$$K_{\pm 2}(l,l') = \sum_{l''} g_{l''}^2 \frac{(2l'+1)(2l''+1)}{32\pi^2} W^2(l,l',l'')(1 \pm (-1)^{l+l'+l''}) \ . \tag{3}$$

Here g_l are found by the inverse Legendre transform of the Gabor window $G(\theta,\phi)$ and the Wigner symbols W are defined as:

$$W(l,l',l'') = \begin{pmatrix} l & l' & l'' \\ -2 & 2 & 0 \end{pmatrix} \ . \tag{4}$$

We exploited these formulae for circular cut sky area of different size with top hat shape:

$$G(\theta) = \ 1 \quad \theta \leq \theta_C \ , \tag{5}$$

$$G(\theta) = \ 0 \quad \theta > \theta_C \ . \tag{6}$$

As one can see from equations (1) and (2), the cut causes a mix of the polarization E and B modes, due to the term $K_{-2}(l,l')$. Obviously, the mixing gets reduced as the size of the window is increased. Since the cosmological fluctuations are dominated by the scalar contribution in the cosmological concordance model (Spergel et al. 2003), even if the diagonal of the kernel $K_2(l,l')$ is one order of magnitude larger than the diagonal of $K_{-2}(l,l')$, we expect the E mode to contaminate substantially the B signal even for large regions of the sky, while on the other hand $\tilde{C}_l^E \simeq C_l^E$.

In Fig.4 we show the pseudo power spectrum of the B mode, $\tilde{C}_l^B$, as defined in (2) for a top hat window with $\theta_C = 10^\circ$ and 20°. In the latter case, the leakage from the E modes is slightly weaker. We limit our analysis to a maximum $l = 1000$ just for a computational convenience in term of speed for calculating the pseudo-C_ls. We keep this limit also in the analysis in the next sections. For comparison the dashed line are the full sky B modes (with power normalized on the patch). As we see, the shapes of the two spectra are substantially different and the E mode contamination is relevant in the pseudo-C_l^B. The leakage in the B component is maximum where the E power is larger; as a consequence, on the degree scale corresponding to the bump from gravitational waves, the latter is still visible in the pseudo-C_l^B. In the following sections, we shall quantify the quality of the reconstruction in the angular domain, on the basis of the pseudo power spectrum.

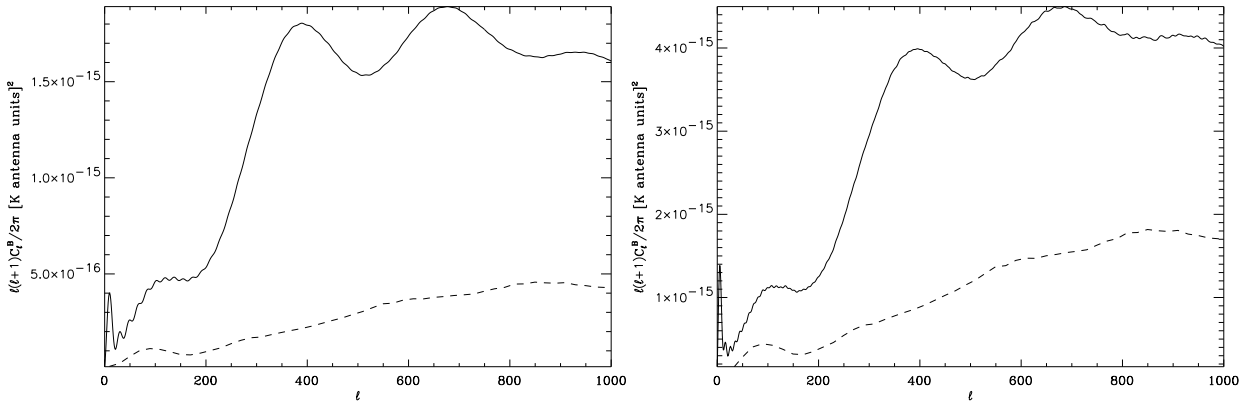

Figure 4. Pseudo power spectra for the B modes, in the case of a circular top hat cut of $\theta_C = 10^\circ$ (left panel, solid line) and $\theta_C = 20^\circ$ (right panel, solid line). The dashed lines in both panels represent the full sky C_l^B normalized to the patch area fractions. The contamination due to the E mode is evident.

4 COMPONENT SEPARATION

In this Section we present a first application of the lightICA code, based on FastICA, optimized for parallel runs and operating on polarization data. We first describe the basic features of the algorithm, then show its performance on our simulated data. We do not report here all the details of the FastICA technique, as they may be found in earlier works, concerning total intensity (Maino et al. 2002) and polarization (Baccigalupi et al. 2004). As described above, we consider here two frequency combinations, 40 and 90 GHz, 150 and 350 GHz, where the CMB is contaminated by synchrotron and dust diffuse polarized emission, respectively. The CMB is added to the foregrounds at the different frequencies in Q and U, expressed in Kelvin antenna units. We adopt a spatial resolution of about $3.5'$ arcminutes, corresponding to $n_{side} = 1024$ resolution parameter in the HEALPix scheme. Before processing, all the maps have been smoothed with a Gaussian, circular beam with full width half maximum (FWHM) equal to 10 arcminutes; moreover, a Gaussian and uniformly distributed noise is added, with amplitude specified below. As we stress in the following, the high resolution is a crucial requirement for a successful application of the ICA techniques, as they do not rely on other prior than the statistical independence of the signal to reconstruct, and need a large number of realizations to converge to the solution. The spatial resolution considered here is actually close to the target for the forthcoming experiments (Montroy et al. 2004; Bowden et al. 2004; Oxley et al. 2004), as a large part of the signal expected for the B modes of the CMB, i.e. the lensing peak, is relevant on those scales.
In all the cases we show, a single separation run (not including the construction of the simulated sky) takes about 5 seconds on a workstation with 1.5 Gb RAM and 2.4 GHz Pentium IV processor.

4.1 lightICA: an MPI parallel implementation of the FastICA component separation in polarization

As discussed in detail recently (Baccigalupi et al. 2004), the FastICA technique can be applied to polarization measurements operating on the Q and U Stokes parameter. On all sky, Q and U may be combined to get the E and B modes (Zaldarriaga, Seljak 1997; Kamionkowski et al. 1997); as discussed in Section 3, when a fraction of the sky is considered, a mixing between E and B modes occurs. The ICA technique consists mainly in a maximization of an approximation of the neg-entropy, measuring the distance of a mixture of signals from a Gaussian distribution (Amari, Chichocki 1998; Hyvärinen 1999). The hypothesis are that the mixture contains at most one Gaussian component and that all of them obey different probability distributions and frequency scalings; if this is verified, it is possible to demonstrate that asymptotically in the number of realizations (pixels in our case), the local maxima of the neg-entropy correspond to the components present into the mixture. The excellent performance obtained so far on simulated CMB data is due mainly to two features: the good detail in the maps, reaching the arcminute scale, as well as the high level of independence between the background CMB and the foreground emissions (Maino et al. 2002; Baccigalupi et al. 2004).
Due to these promising results, and in view of the application to real polarization data, it is now necessary to build a machinery capable of evaluating the errors in the separation as well as the stability of its quality against variation of the main unknowns entering a given dataset, such as instrumental noise, CMB realizations, foreground properties, area covered by a given experiment and so on. Along with pure theoretical studies, these issues may be quantified implementing suitable Monte Carlo simulations. Due to the remarkable speed of a single ICA component separation run, such technique is particularly suited for parallelization. In the lightICA code, the main ICA routine, dealing basically with arrays of numbers, is called by each processor dealing with its own version of the sky. The code consists in a main driver performing the following steps. A

number of CMB realizations is pre-computed and a set of external variables determine the case under study, namely set of frequencies, foreground fluctuation amplitude, noise amplitude, etc. For each CPU, the driver performs a first, purely mathematical operation generating random numbers in order to initialize the noise data streams. Then it calls a separate routine summing up the different components in the sky, in an HEALPix format, separately for the Q and U Stokes parameters, by making use of the external variables. Let $\mathbf{x}^Q$ and $\mathbf{x}^U$ be the multi-frequency data, where $\mathbf{x}$ is made of two indexes, labeling frequencies on rows and pixels on columns. The algorithm assumes that the components scale rigidly in frequency, which means that each of them can be represented by a product of two functions depending on frequency and space separately; we can define a spatial pattern for them, which we indicate with $\mathbf{s}^Q$ and $\mathbf{s}^U$. Then we can express the inputs $\mathbf{x}^{Q,U}$ as

$$\mathbf{x}^{Q,U} = \mathbf{A}^{Q,U}\,\mathbf{s}^{Q,U} + \mathbf{n}^{Q,U}\ , \tag{7}$$

where the matrices $\mathbf{A}^{Q,U}$ scale the spatial patterns of $\mathbf{s}^{Q,U}$ to the input frequencies; the instrumental noises $\mathbf{n}^{Q,U}$ have same dimensions as $\mathbf{x}$. Note that equation (7) implies that all the frequencies has the same spatial resolution, which is not the case in real observations and is actually a limitation of the ICA technique on the real space, requiring to work at the lowest resolution of a given experiment.

The constructed skies are given as inputs to the main ICA core routine performing the actual separation. The maximization of the neg-entropy produces two separation matrices, $\mathbf{W}^Q$ and $\mathbf{W}^U$, producing a copy of the independent components present in the data:

$$\mathbf{y}^Q = \mathbf{W}^Q\mathbf{x}^Q\ \ ,\ \ \mathbf{y}^U = \mathbf{W}^U\mathbf{x}^U\ . \tag{8}$$

All the details on the way the separation matrix for FastICA is estimated are given in previous works (Maino et al. 2002; Baccigalupi et al. 2004), together with a recipe to recover the frequency scaling of the signals $\mathbf{s}^{Q,U}$. Then $\mathbf{y}^Q$ and $\mathbf{y}^U$ can be combined together to get the E and B modes of each reconstructed component. Note that the noise correlation matrix can be taken into account in the separation process; this is done simply by subtracting the noise correlation matrix from the one of the total signal before entering into the core of the algorithm (Hyvärinen 1999); for an uniform and Gaussian distributed noise, its correlation matrix is null except on the diagonal, containing the noise variances at the frequencies considered. However, note that even if separation goes perfect, equations (7,8) imply that the noise is transmitted to the outputs:

$$\mathbf{n}_y^{Q,U} = \mathbf{W}^{Q,U}\mathbf{n}^{Q,U}\ . \tag{9}$$

This means that, if the noises on different channels are uncorrelated and Gaussian, and indicating as σ_{ν_j} the input noise root mean square (*rms*) at frequency ν_j, the noise *rms* on the i-th output is

$$\sigma_{y_i}^{Q,U} = \sqrt{\sum_j |W_{ij}^{Q,U}|^2 |\sigma_{\nu_j}^{Q,U}|^2}\ . \tag{10}$$

For full sky signals, the noise contamination to the angular power spectrum is $C_{l,\,n_i}^{Q,U} = 4\pi(\sigma_{y_i}^{Q,U})^2/N$, where N is the number of pixels. Gaussianity and uniformity make also very easy to calculate the noise level on E and B modes, since they contribute at the same level: $C_{l,\,n_i}^{E} = C_{l,\,n_i}^{B} = (C_{l,\,n_i}^{Q} + C_{l,\,n_i}^{U})/2$. The latter quantities represent the average noise power, which can be simply subtracted from the output power spectra by virtue of the uncorrelation between noise and signal. The remaining uncertainty comes from noise realization, which at 1σ is: $\Delta C_{l,\,n_{(i)}}^{E,B} = \sqrt{2/(2l+1)}C_{l,\,n_i}^{E,B}$.

The final step consists in the output of the results. Those may be in the form of maps or power spectra, computed simply with the HEALPix routines. The code also outputs the separation matrix and its inverse as computed by each processor.

The overall structure of the lightICA is rather flexible; in particular, the header dealing with different variables may be easily changed and specialized for studying a particular degree of freedom. It is also quite extensible and, for example, the openMP HEALPix routines can be easily incorporated if a further speed-up of the power spectrum computation is desired.

In the following we present the first applications of lightICA. We choose and analyze a suitable reference simulated dataset, and then we study the stability of the results against variation of some among the most relevant degrees of freedom of the simulated dataset. In each case, the separation quality is quantified by the ICA induced bias and additional uncertainty of the recovered CMB spectra as evaluated in each Monte Carlo series.

4.2 B modes reconstruction and error estimation

The sky signals in the patch considered are processed to the lightICA code, and the outputs, in E and B, are shown in figures 5, 6, and 7, 8, respectively. Those are plotted at 40 and 150 GHz in antenna units, as the code outputs are at the lowest frequency by default. In each panel, the two dotted curves correspond to the theoretical pseudo-$C_l^{E,B}$ of the CMB signal, $\pm 1\sigma$ where σ represents the cosmic variance on our patch of the sky: that is specified by a fraction f_{sky} and binned over $\Delta l = 50$ multipoles (Tegmark 1997), and is given by

$$\Delta\tilde{C}_l^{E,B} = \sqrt{\frac{2}{(2l+1)\Delta l f_{sky}}}(\tilde{C}_l^{E,B} + \tilde{C}_{n,l}^{E,B}) \ , \tag{11}$$

where $\tilde{C}_{n,l}^{E,B}$ are the contribution of the noise. At the bottom of each figure, we also plot the average and standard deviation of the residuals, obtained by subtracting the input from the output pseudo-power spectra for each realization. We assume a Gaussian and uniformly distributed noise over the analyzed region, with *rms* equal to a half of that of the CMB ($S/N = 2$), at each frequency. The noise amplitude is not related to any particular experiment, and was chosen as a starting point for the analysis performed in the next sub-section, where the noise amplitude is varied. Note that, on the all sky, the chosen noise amplitude is shown in figure 1.

The error bars represent the signal recovered by the LIGHTICA separation process, plus and minus the 1σ uncertainty obtained by performing a hundred Monte Carlo simulations over the CMB realization and noise. Thus, it represents the error in the separation process, given the foreground templates assumed in this work. On the other hand, the residuals give a measure of the faithfulness of the reconstruction on each realization. Since on the residuals the cosmic variance uncertainty is absent, the precision decrease on high multipoles, visible mostly on B modes, is due to the noise sample variance.

The first feature to be noted is that the separation is clearly successful, for E and B as well. Note that the latter are generally comparable or lower than the foreground and noise contamination, as we show explicitly in the next sub-section. As we stressed above, the ICA technique looks for the independent components into the data, assuming rigid and different frequency scaling and a different statistics for all of them, with no other prior; the fact that this procedure is able to extract with precision a signal which is comparable or lower than the foreground contamination in presence of noise is remarkable. Once again, the latter performance is made possible by the good detail in the data, the arcminute scale, as well as the high level of statistical independence between background and foreground emission. These two occurrences bring the algorithm close to an ideal environment, making it converging close to the right result, with a precision represented by the errors shown in the figures.

A second, most interesting aspect to be noted is that we detect the error due to the separation process; that is clearly visible in all the figures as the excess in the error bars with respect to what predicted by cosmic variance and noise. The error from component separation is comparable or smaller, indicating a simple, linear response of the ICA algorithm to the sample variance of the simulated templates. The error may be due to the following reasons. First, as stressed in section 4.1, the noise correlation matrix is subtracted from the one of the total signal before the separation process. Thus, the signal correlation matrix remains affected by the noise only through the uncertainty due to its realization in the actual data. Second, on a single realization, background and foreground are not completely independent. This introduces a random bias in the ICA performance, which may contribute to the separation error.

Another interesting feature may be noted by looking at figure 8, showing an excess power in the recovered spectra and residuals with respect to the input ones, mostly concentrated at low multipoles. This occurrence is interpreted not in terms of the different pattern of the foreground emission for dust and synchrotron, but in terms of the relative weight of it with respect to the background emission, as already noticed in earlier works (Maino et al. 2002; Baccigalupi et al. 2004). Due to the difference in the frequency scalings in the bands considered, in the 40, 90 GHz case the foreground and background signals are closer in amplitude with respect to the higher frequency combination; thus, at 150 GHz the CMB dominates over the dust while at 350 GHz the CMB emission is negligible. Indeed, this bias disappears if the foreground amplitude is raised by a factor of a few.

Finally, note that our Monte Carlo analysis does not include variations in the foreground template, which should be included as well in order to quantify properly the error in the separation process. Indeed, the modest knowledge of the foreground emissions available does not allow to estimate their statistics to a level high enough to vary their template into the Monte Carlo.

4.3 Varying noise, foreground amplitudes and analyzed area

We perform here a first study of the results variation when some key parameters of the simulations are varied. Specifically, we vary noise amplitude, foreground fluctuation amplitude and extension of the sky area considered. Moving along the "directions" of this parameter space, we are able to give constraints on the applicability of the LIGHTICA process in a systematics free enviroment and given the foreground pattern assumed.

In order to quantify the error introduced by the algorithm with respect to the one associated with cosmic variance and noise, we introduced the following quantities:

$$b_l = \frac{\langle\tilde{C}_l^{E,B}\rangle_{\rm ICA} - \tilde{C}_l^{E,B}}{\Delta\tilde{C}_l^{E,B}}, \tag{12}$$

$$r_l = \frac{\langle\Delta\tilde{C}_l^{E,B}\rangle_{\rm ICA}}{\Delta\tilde{C}_l^{E,B}}, \tag{13}$$

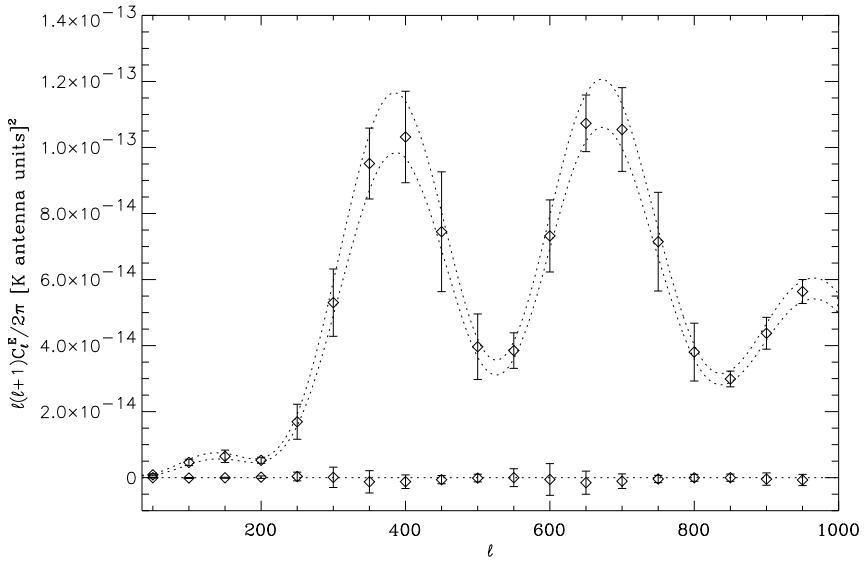

Figure 5. Pseudo-power spectra of the reconstructed $\tilde{C}_l^E$ modes of the CMB in the 40, 90 GHz frequency combination, in the $S/N = 2$ case. The region between the dotted lines is the theoretical CMB signal $\pm\sigma$ cosmic and noise variance at 40 GHz on the sky area considered. At the bottom we show the average and standard deviation of the residuals on each realization.

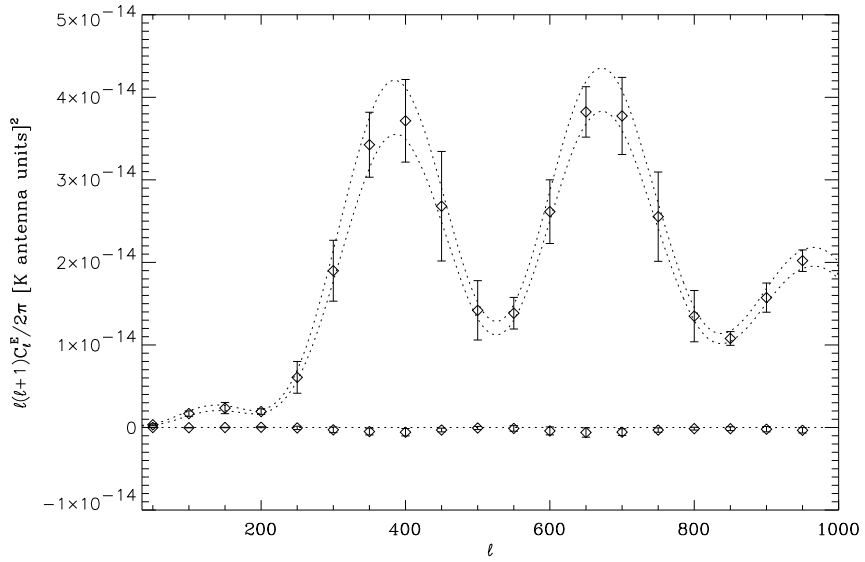

Figure 6. Pseudo-power spectra of the reconstructed $\tilde{C}_l^E$ modes of the CMB in the 150, 350 GHz frequency combination, in the $S/N = 2$ case. The region between the dotted lines is the theoretical CMB signal $\pm\sigma$ cosmic and noise variance at 150 GHz on the sky area considered. At the bottom we show the average and standard deviation of the residuals on each realization.

where the $\langle\rangle$ represents the average over all the realizations and the denominator is given by (11). Those are, respectively, the bias and the extra uncertainty, which both quantify the imperfectness of the foreground removal process and are defined with respect to the theoretical $\tilde{C}_l^{E,B}$. They allow us to attempt to give a definition for a "successful" separation, which is when the LIGHTICA is able both to recover the CMB signal, i.e. to produce small biases, and to keep the value of the ratio r_l close to unity. In tables 1 and 2, we report the values of these quantities for some relevant multipoles as a function of the varying parameters.

We begin varying the noise with respect to the simulated dataset considered in the previous sub-section. We found out the results to be very stable up to $S/N = 1$. As it may be noted by looking at the tables, the algorithm performance does not exhibit any noticeable degradation from the noiseless case up to $S/N = 1$. Beyond this point, the code starts failing to

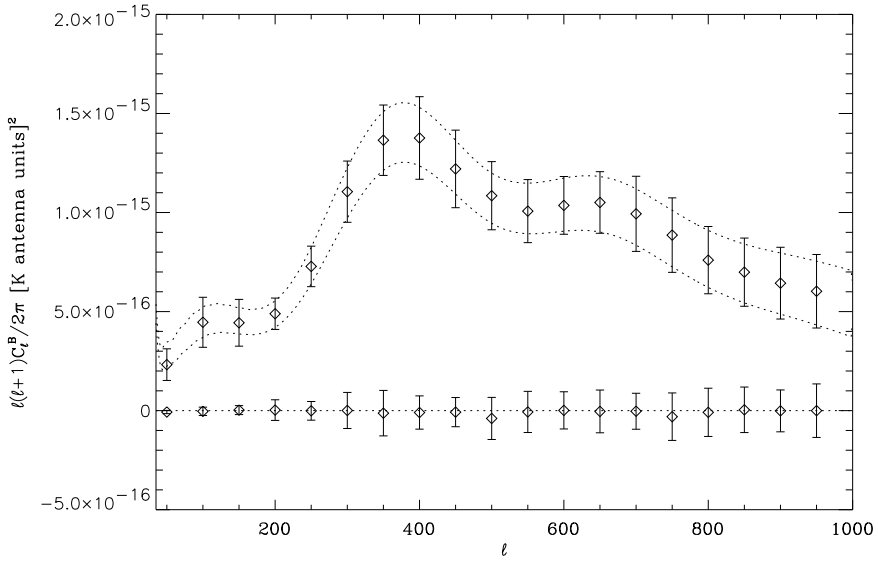

Figure 7. Pseudo-power spectra of the reconstructed $\tilde{C}_l^B$ modes of the CMB in the 40, 90 GHz frequency combination, in the $S/N = 2$ case. The region between the dotted lines is the theoretical CMB signal $\pm\sigma$ cosmic and noise variance at 40 GHz on the sky area considered. At the bottom we show the average and standard deviation of the residuals on each realization.

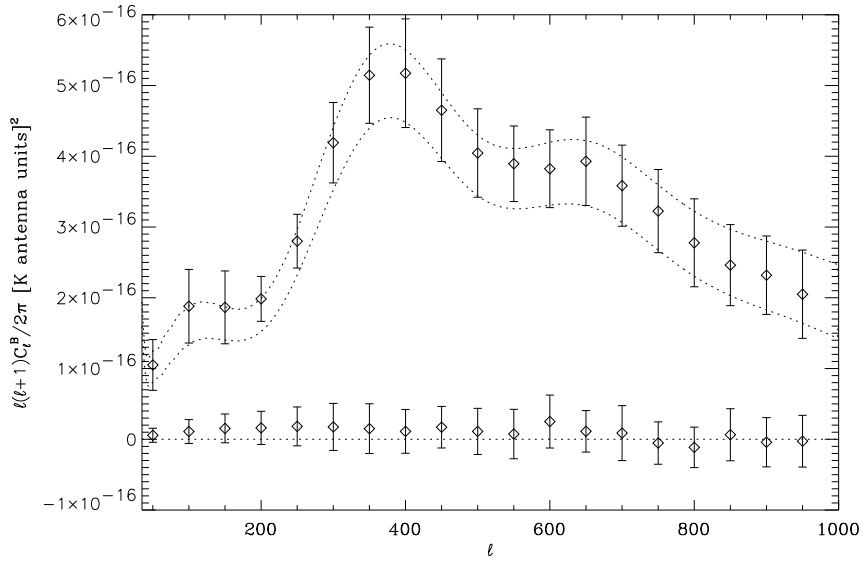

Figure 8. Pseudo-power spectra of the reconstructed $\tilde{C}_l^B$ modes of the CMB in the 150, 350 GHz frequency combination, in the $S/N = 2$ case. The region between the dotted lines is the theoretical CMB signal $\pm\sigma$ cosmic and noise variance at 150 GHz on the sky area considered. At the bottom we show the average and standard deviation of the residuals on each realization.

reconstruct the signals, first via a leakage of the foreground pattern into the reconstructed B modes of the CMB, then not converging at all or finding negative eigenvalues in the signal correlation matrix caused by the noise sample variance.
The foreground variation is realized by leaving the mean on the area considered unaffected, increasing the *rms* only, by a factor 2, 4, 6 for synchrotron, and even 10 for dust. In figures 9 and 10 we report the foreground B modes at 40, 90 GHz and 150, 350 GHz, respectively, for the *rms* considered. For reference, we also plot the theoretical CMB pseudo-spectra. At 40 and 350 GHz, the contamination to the CMB is worse of course. Despite the high level of foreground fluctuations, the code exhibits again a remarkable stability in the interval considered for this parameter; it starts failing only when the foreground *rms* is increased by a factor of about 6 for synchrotron, and by a factor of about 10 for dust. This occurrence may be interpreted as follows. The separation degradation due to the increased foreground fluctuation amplitude is compensated by the fact that

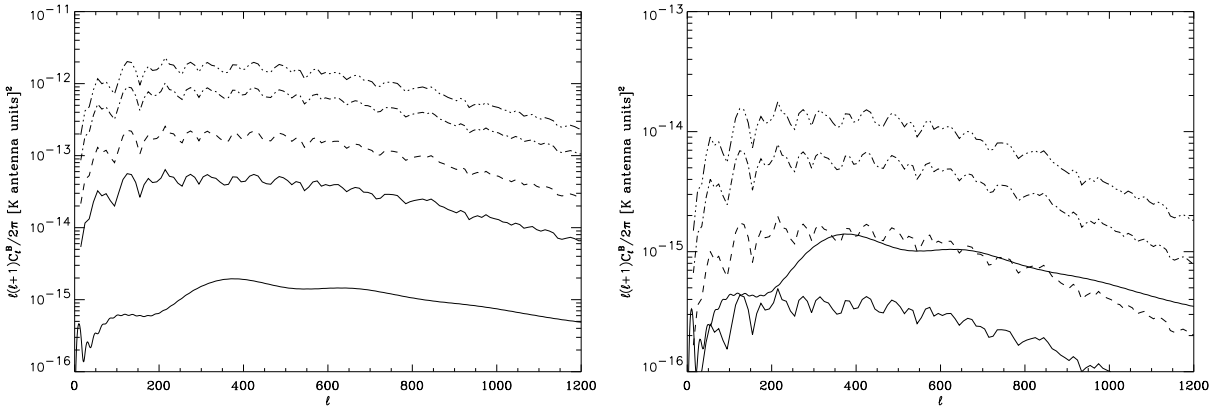

Figure 9. Pseudo-power spectra of the synchrotron B modes calculated for the sky region and with the amplitudes as considered in this work, at 40 (left) and 90 GHz (right). The different curves, with raising power, correspond to the foreground *rms* multiplied by 1, 2, 4, and 6, respectively. In each panel the solid smoothed line represents the B modes of the CMB.

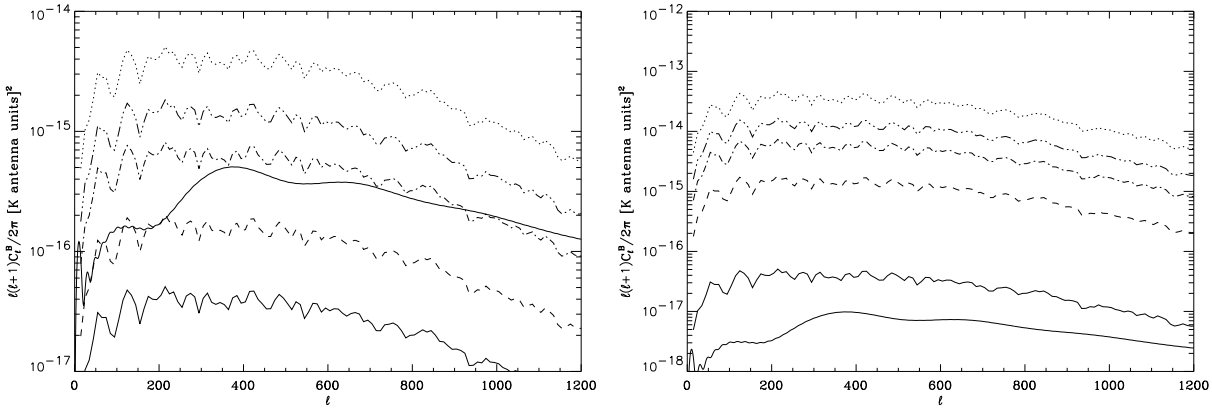

Figure 10. Pseudo-power spectra of the dust B modes calculated for the sky region and with the amplitudes as considered in this work, at 150 (left) and 350 GHz (right). The different curves, with raising power, correspond to the foreground *rms* multiplied by 1, 2, 4, 6 and 10, respectively. In each panel the solid smoothed line represents the B modes of the CMB.

the foregrounds itself get higher than the noise, making their recovery easier; indeed, for an ICA base component separation technique where the only mean of the algorithm is the mutual independence of the components to be recovered, the quality in the reconstruction of each of them depends on how well the other ones are extracted (Maino et al. 2002; Baccigalupi et al. 2004).

As it may be noted in the tables, things worsen a bit after doubling the radius of the cut. We interpret this result in the following way. As shown by Maino et al. (2002), the best work conditions for ICA are met with signals which are uniformly distributed; by enlarging the area covered, the foregrounds get inhomogeneous. In other words, since the patch with $\theta_C = 10$ degrees has already a large number of samples (pixels), the net effect of increasing θ_C is not to add statistics, but just to make the foregrounds not uniform; in particular, for $\theta_C = 20$ degrees, the dust template exhibits a localized hot spots dominating over the other features.

In the tables we also report the maximal values that r_l and b_l assumed in the different separation cases in the range of l stretching from 50 to 1000. It can be noticed that the worst performance of the algorithm is usually seen at $l_{max} \sim 150 - 200$. This is because the separation process is more likely to leave more pronounced residuals at the angular scales where the foreground emission is the highest with respect to the amplitude of the CMB signal (see figures 9 and 10).

As a final remark, we notice that increasing the noise amplitude, the reconstruction is less accurate when the dust is taken into account. As we anticipated in Section 4.2, this is due to the fact that at 150 GHz, the dust emission is negligible with respect to CMB and noise. Indeed, as noticed in earlier works (Maino et al. 2002; Baccigalupi et al. 2004), the separation is more accurate when the signals are comparable in all frequency bands. This is supported by the fact that the performance improves

S/N	Fore. Ampl.	Cut Radius	$r_{l=100}$ Synchr.	$b_{l=100}$ Synchr.	$r_{l=400}$ Synchr.	$b_{l=400}$ Synchr.	$r_{l=950}$ Synchr.	$b_{l=950}$ Synchr.	max(r_l) Synchr.	max(b_l) Synchr.
∞	1.00	10	1.74	-0.08	1.69	-0.06	1.49	0.04	2.03 ($l_{max} = 150$)	0.13 ($l_{max} = 200$)
2.00	1.00	10	1.64	-0.06	1.41	-0.08	1.15	0.04	1.79 ($l_{max} = 150$)	0.24 ($l_{max} = 200$)
1.50	1.00	10	1.58	-0.02	1.29	-0.06	1.14	0.08	1.67 ($l_{max} = 150$)	0.29 ($l_{max} = 200$)
1.00	1.00	10	1.52	0.22	1.12	0.10	1.02	0.04	1.52 ($l_{max} = 100$)	0.57 ($l_{max} = 200$)
2.00	2.00	10	1.62	-0.12	1.46	0.06	1.19	0.16	1.80 ($l_{max} = 150$)	0.20 ($l_{max} = 200$)
2.00	4.00	10	1.60	-0.12	1.82	0.50	1.25	0.40	1.83 ($l_{max} = 150$)	0.55 ($l_{max} = 350$)
2.00	6.00	10	1.60	-0.16	1.62	0.66	1.32	0.54	1.84 ($l_{max} = 150$)	0.66 ($l_{max} = 400$)
2.00	1.00	20	2.02	0.26	1.75	0.18	1.47	-0.16	2.21 ($l_{max} = 150$)	0.89 ($l_{max} = 200$)

Table 1. Relative extra uncertainty, r_l, and bias, b_l, calculated for the cosmological B-mode power spectrum. These are due the synchrotron signal assumed in the analyzed maps and subsequently removed applying the FastICA algorithm, prior to the power spectrum computation. The results are given for three different values of the multipole l together with the maximal values found for a range of l from 50 to 1000, and for multiple choices of the sky and noise parameters as listed in the table.

S/N	Fore. Ampl.	Cut Radius	$r_{l=100}$ Dust	$b_{l=100}$ Dust	$r_{l=400}$ Dust	$b_{l=400}$ Dust	$r_{l=950}$ Dust	$b_{l=950}$ Dust	max(r_l) Dust	max(b_l) Dust
∞	1.00	10	1.92	0.74	1.64	0.28	1.53	0.38	2.44 ($l_{max} = 150$)	1.29 ($l_{max} = 200$)
2.00	1.00	10	1.90	0.90	1.50	0.30	1.24	-0.18	2.21 ($l_{max} = 150$)	1.18 ($l_{max} = 200$)
1.50	1.00	10	1.92	1.26	1.45	0.40	1.24	-0.30	2.25 ($l_{max} = 150$)	1.57 ($l_{max} = 150$)
1.00	1.00	10	2.25	2.70	1.52	0.96	1.26	0.42	2.71 ($l_{max} = 150$)	3.19 ($l_{max} = 200$)
2.00	2.00	10	1.79	0.58	1.52	0.14	1.16	-0.32	2.11 ($l_{max} = 150$)	0.92 ($l_{max} = 150$)
2.00	4.00	10	1.82	0.62	1.49	0.14	1.17	-0.28	2.13 ($l_{max} = 150$)	0.91 ($l_{max} = 150$)
2.00	6.00	10	1.80	0.58	1.50	0.16	1.17	0.28	2.18 ($l_{max} = 150$)	0.94 ($l_{max} = 150$)
2.00	10.00	10	2.00	0.56	2.04	0.44	1.50	-0.14	2.31 ($l_{max} = 150$)	0.91 ($l_{max} = 150$)
2.00	1.00	20	3.51	1.50	3.05	0.82	2.21	0.46	3.82 ($l_{max} = 150$)	1.83 ($l_{max} = 200$)

Table 2. As Table 1, but for the cases considering the dust as the foreground emission.

or remains unaltered when the dust fluctuation amplitude is increased while in the synchrotron case, a clear degradation of the separation may be seen.

5 DISCUSSION

In this work we discuss the performance of the component separation technique based on the Independent Component Analysis (ICA) as applied to the small patches of the polarized sky observed in the microwave band. We focus on the recovery of the Cosmic Microwave Background (CMB) signal out of the contamination due to the diffuse foreground emission from the Galaxy and perform a Monte Carlo analysis to estimate the resulting errors. These computations employ lightICA – a newly developed parallel implementation of the FastICA code (Hyvärinen 1999; Maino et al. 2002). The sky region considered is the target of several CMB experiments as it is known to feature a low foreground emission in total intensity. On the other hand, the current knowledge of the foreground emission indicates that the contamination to the CMB emission in polarization might be relevant in any region of the sky, and at any frequency considered. This is true in particular for the component of the CMB signal due to the primordial gravitational waves and lensing mechanisms (B modes); the latter signal is extremely relevant in modern cosmology as it may demonstrate the existence of gravitational waves of cosmological origin, as well as reveal crucial clues about the structure formation in the universe.

The idea behind the ICA is based on the assumption that the background and foreground statistics are indipendent, requiring

no other prior on the signals to recover, on their pattern or frequency scaling. All the available data and simulations on the Galactic foreground emission indicate that the CMB and Galactic emission are highly statistical independent; indeed, the CMB is known to have a statistics which is close to the Gaussianity, while the Galaxy is known to be highly non-Gaussian. This occurrence, together with the high level of detail in the present CMB data, reaching the arcminute scale, allow the ICA technique to recover the CMB pattern extremely close to the actual one.
We consider two frequency bands where the foreground contamination is given by the synchrotron and the thermal dust, respectively, and we assume a Gaussian and uniform noise distribution with amplitude comparable to the total CMB polarized emission. We quantify the quality of the reconstruction by comparing the input and output angular power spectra on the sky fraction which we consider (pseudo power spectra). Due to its parallelized structure, the LIGHTICA allows to evaluate the error in the separation process on each relevant angular scale, exploiting Monte Carlo series varying some of the most relevant degrees of freedom entering in the dataset simulation. We identify the error induced by the separation process on the CMB reconstruction and show that is comparable or lower than the uncertainty given by the instrumental noise. We remark that in terms of B modes, this is achieved in presence of a foreground contamination which may be several times stronger than the cosmological signal, which has been simulated accordingly to the current polarized foreground models. Then, we evaluate the stability of these results against variation of the noise and foreground fluctuation amplitude, as well as the sky area covered. We find considerable intervals of these parameters where the results, in terms of reconstruction of B modes, do not change substantially. In particular, the claim that the error induced by the reconstruction is of the order of the cosmic plus noise sample variance, remains true in all these cases. Moreover, the outputs exhibit a remarkable stability for a large foreground fluctuation amplitude, several times larger than predicted by the current foreground models; this may be due to a compensation between the degradation which would be induced by the large foreground signal, and the fact that the latter is better extracted as it gets larger over the noise. Finally, we found that increasing the area covered yields a degradation of the outputs, as expected since the foregrounds gets less and less uniformly distributed.

We have not considered any specific planned or on-going experiment, but rather focused on a handful of important but quite general and basic parameters. This is because our aim is to show that if the foreground contamination to the B modes of the CMB turns out to be consistent as the current foreground models predict, then an ICA based component separation may be required and adequate to achieve the detection of the cosmological signal. It is still premature to attempt a quantitative estimation of the ICA nominal performance taking into account the uncertainty in the foreground signal, in general or for a given experiment. Indeed, the available information on the Galactic polarized signal is still too modest to assess properly its statistical distribution.
Moreover, it is useful to recall the ICA fundamental hypotheses and limitations at the present level of the code architecture. Together with the statistical independence, which is likely to be very well verified for the CMB and the Galaxy, a fundamental limitation is represented by the assumption that the signals scale rigidly in frequency, which means that the spectral index is spatially independent. This is not verified on the whole sky, as both the energy distribution of free electrons, as well as the thermal dust temperature, exhibit fluctuations. On the other hand, so far there is no evidence that the synchrotron spectral index actually vary substantially on the angular scales considered in experiments observing a limited fraction of the sky, which is usually comparable to a percent of the sky. In addition, in the real space the ICA requires to work at the same angular resolution at all frequencies, which is not the case for most of the operating of planned observations. This makes necessary to work at the lowest resolution, or an approach in the harmonic space should be implemented. Ultimately, the stability of the performance in nominal conditions has to be quantified and verified in presence of instrumental systematics, such as non-uniform and non-gaussian noise, beam asymmetry, etc.

However, we believe that the excellent performance shown here justifies the interest and effort toward the implementation of techniques based on the Independent Component Analysis in real experimental conditions. Even if only a fraction of their capability remains in a real experiment application, that might be crucial in order to measure the actual pattern of the curl component of the CMB polarized emission.

ACKNOWLEDGEMENTS

Carlo Baccigalupi is grateful to George F. Smoot for several useful discussions. Some of the results in this paper have been derived using the Hierarchical Equal Area Latitude Pixelization of the sphere (HEALPix, Górski, Hivon and Wandelt 1999). The theoretical power spectra were calcualted using the CMBFAST software by Seljak, Zaldarriaga (1996). We acknowledge the use of National Energy Research Scientific Computing Center computing resources. This research was supported in part by the NASA LTSA grant NNG04GC90G.

REFERENCES

Amari S., Chichocki A., 1998, *Proc. IEEE* 86, 2026

Baccigalupi C. et al., 2000, *MNRAS* , 318, 769
Baccigalupi C. et al., 2001, *Astron. & Astrophys.* 372, 8
Baccigalupi C., 2003, *New Astron. Rev.* 47, 1127
Baccigalupi C., 2004, *MNRAS* 354, 5570
Bennett C.L. et al., 2003, *Astrophys. J. Supp.* 148, 97
Benoit A. et al., 2004, *Astron. & Astrophys.* 424, 571
Carretti E., Bernardi G., Sault R.J., Cortiglioni S., Poppi S., 2005 *MNRAS* in press, preprint, `astro-ph/0412598`
Bouchet F.R., Prunet S., Sethi S.K., 1999, *MNRAS* , 302, 663
Bowden M. et al., 2004, *MNRAS* 349, 321
Brouw W.N., Spoelstra T.A.T., 1976, *Astron. & Astrophys. Suppl.* 26, 129
Chon, G., Challinor A., Prunet S., Hivon E. Szapudi I., 2004, *MNRAS* 350, 914
De Zotti G., Gruppioni C., Ciliegi P., Burigana C., and Danese L., 1999, *New Astron.* 4, 481
Delabrouille J., Cardoso J.F., Patanchon G., 2003, *MNRAS* 346, 1089
Duncan A.R., Reich P., Reich W., Fürst E., 1999, *Astron. & Astrophys.* 350, 447
Finkbeiner D.P., Davis M., Schlegel D.J. 1999, *Astrophys. J.* 524, 867
Gabor D., 1946, *J. Inst. Elect. Eng.* 93, 420
Giardino G. et al., 2002, *Astron. & Astrophys.* 387, 82
Hansen F.K., Górski K.M., Hivon E., 2002, *MNRAS* 336, 1304
Haslam C.G.T., Stoffel H., Salter C.J., Wilson W.E., 1982, *Astron. & Astrophys. Suppl.* 47, 1
Hyvärinen A., 1999, *IEEE Signal Processing Lett.* 6, 145
Hobson M.P., Jones A.W., Lasenby A.N., Bouchet F., 1998, *MNRAS* 300, 1
Jones T.J., Klebe K., Dickey J.M., 1992, *Astrophys. J.* 389, 602
Kamionkowski M., Kosowsky A., Stebbins A., 1997, *Phys. Rev. D* 55, 7368
Kogut A. et al., 2003, *Astrophys. J. Supp.* 148, 161
Kovac J. et al., 2002, *Nature* 420, 772
Lewis A., 2005, *Phys. Rev. D* 71, 083008
Maino D. et al., 2002, *MNRAS* 334, 53
Maino D., Banday A.J., Baccigalupi C., Perrotta F., Górski K., 2003, *MNRAS* 344, 544
Mesa D. et al., 2002, *Astron. & Astrophys.* 396, 463
Montroy T. et al., 2004, *New Astron. Rev.* 47, 1057
Oxley P. et al., 2004, Earth Observing Systems IX. Edited by William L. Barnes and James J. Butler, Proceedings of the SPIE, 5543, 320
Prunet S., Sethi S.K., Bouchet F.R., Miville-Deschenes M.A., 1998, *Astron. & Astrophys.* 339, 187
Readhead A.C.S., 2004, *Science* 306, 836
Sazonov S.Y., Sunyaev R.A., 1999, *MNRAS* 310, 76
Seljak U., Hirata C.M., 2004, *Phys. Rev. D* 69, 043005
Seljak U., Zaldarriaga M., 1996, *Astrophys. J.* 469, 437
Smith K.M., Hu W., Kaplinghat M., 2004, *Phys. Rev. D* 70, 043002
Spergel D.N. et al., 2003, *Astrophys. J. Supp.* 148, 175
Stolyarov V., Hobson M.P., Ashdown M.A.J., Lasenby A.N., 2002, *MNRAS* 336, 97
Tegmark M., 1997, *Phys. Rev. D* 55, 5895
Tegmark M., Efstathiou G., 1996, *MNRAS* 281, 1297
Tucci M., et al., 2002, *Astrophys. J.* 579, 607
Uyaniker B., Fürst E., Reich W., Reich P., Wielebinski R., 1999, *Astron. & Astrophys. Suppl.* 138, 31
Zaldarriaga M., 2001, *Phys. Rev. D* 64, 103001
Zaldarriaga M., Seljak U., 1997, *Phys. Rev. D* 55, 1830
Zaldarriaga M., Seljak U., 1998, *Phys. Rev. D* 58, 023003